

Surface Scattering Expansion of the Casimir-Polder Interaction for Magneto-dielectric Bodies: Convergence Properties for Insulators, Conductors and Semiconductors

Giuseppe Bimonte ^{1,†} and Thorsten Emig ²

¹ Dipartimento di Fisica E. Pancini, Università di Napoli Federico II, Complesso Universitario di Monte S. Angelo, Via Cintia, I-80126 Napoli, Italy; giuseppe.bimonte@na.infn.it

[†] INFN Sezione di Napoli, I-80126 Napoli, Italy

² Laboratoire de Physique Théorique et Modèles Statistiques, CNRS UMR 8626, Université Paris-Saclay, 91405 Orsay cedex, France

* Correspondence: giuseppe.bimonte@na.infn.it

Abstract: Fluctuation induced forces are a hallmark of the interplay of fluctuations and geometry. We recently proved the existence of a multi-parametric family of exact representations of Casimir and Casimir-Polder interactions between bodies of arbitrary shape and material composition, admitting a multiple scattering expansion (MSE) as a sequence of inter- and intra-body multiple wave scatterings [G. Bimonte, T. Emig, *Phys. Rev. A* 108, 052807 (2023)]. The approach requires no knowledge of the scattering amplitude (T-matrix) of the bodies. Here we investigate the convergence properties of the MSE for the Casimir-Polder interaction of a polarizable particle with a macroscopic body. We consider representative materials from different classes, such as insulators, conductors and semiconductors. Using a sphere and a cylinder as benchmarks, we demonstrate that the MSE can be used to efficiently and accurately compute the Casimir-Polder interaction for bodies with smooth surfaces.

Keywords: Casimir-Polder force, scattering expansion, surface integral equation, Silicon, Gold, Polystyrene

1. Introduction

Following the seminal work of Casimir, who discovered that two discharged perfectly conducting parallel plates at zero temperature attract each other with a force originating from quantum fluctuations of the electromagnetic (em) field [1], Lifshitz successfully used the then new field of fluctuational electrodynamics to compute the Casimir force between two parallel, infinite surfaces of dispersive and dissipative dielectric bodies at finite temperature [2]. By taking the dilute limit for one of the two bodies, Lifshitz could also compute the Casimir-Polder (CP) force between a small polarizable particle and a planar surface. Lifshitz's results remained unsurpassed for a long time, because it was not clear how to extend his computation beyond simple planar surfaces. Computing the Casimir and Casimir-Polder (CP) interactions in non-planar geometries is in fact a notoriously difficult problem, due to the collective and non-additive character of dispersion forces. For a long time the only method to estimate dispersion forces in non-planar setups was the Derjaguin additive approximation [3], the so-called Proximity Force Approximation (PFA), which expresses the Casimir force between two non-planar surfaces as the sum of the forces between pairs of small opposing planar portions of the surfaces. Because of its simplicity, the PFA is still widely used to interpret modern experiments with curved bodies. For reviews, see [4–10].

A significant step forward in the study of curved surfaces was made in the seventies of last century by Langbein, who used scattering methods to study the Casimir interaction between spheres and cylinders [11]. The remarkable work of Langbein went largely unnoticed, and was quickly forgotten. A new wave of strong interest in the problem

Citation: Title. *Physics* 2023, 1, 1–13.
<https://doi.org/>

Received:

Revised:

Accepted:

Published:

Copyright: © 2023 by the authors. Submitted to *Physics* for possible open access publication under the terms and conditions of the Creative Commons Attribution (CC BY) license (<https://creativecommons.org/licenses/by/4.0/>).

arose at the beginning of this century, spurred by modern precision experiments on the Casimir effect [12–20]. The intense theoretical efforts that were put forward culminated in the discovery of the scattering formula [21–23], initially devised for non-planar mirrors [24,25], which expresses the interaction between dielectric bodies in terms of their scattering amplitude, known as T-operator. While this approach has enabled most of recent theoretical progress, the T-operator is known only for highly symmetric bodies, such as sphere and cylinder, or for a few perfectly conducting shapes [26]. Remarkably enough, it has been found that the scattering formula can be computed exactly for the sphere-plate and the sphere-sphere systems, for Drude conductors in the high temperature limit [27,28]. By improved numerical methods, the scattering formula for a dielectric sphere and a plate at finite temperature can be computed with high precision also for experimentally relevant small separations [29]. We note, however, that the precision of current experiments using the simple sphere-plate geometry has not yet reached the point where deviations from the PFA can be observed.

As we said above, the practical use of the scattering approach is limited to the few simple shapes for which the scattering amplitude is known. A more fundamental limitation of the scattering approach is that interlocked geometries evade this method due to lack of convergence of the mode expansion [30]. The necessity of theoretical formulations for a precise force computation in complex geometries has become urgent lately, because recent experiments using micro-fabricated surfaces [30–32] have shown indeed large deviations from the PFA. Theoretical progress has been made for the special case of dielectric rectangular gratings, by using a generalization of the Rayleigh expansion in [33–35]. On a different route, a general semi-analytical approach has been devised for gently curved surfaces, for which a gradient expansion can be used to obtain first order curvature corrections to the proximity force approximation both for the Casimir force [36–39] and for the CP interaction [40,41].

A breakthrough occurred in 2013 [42] when it was shown that surface integral-equations methods [43,44], that have been used for a long time in computational electromagnetism, can be also used to compute, at least in principle, Casimir interactions for arbitrary arrangements of any number of (homogeneous) magneto-dielectric bodies of any shape. The formulation in [42] expresses Casimir forces and energies as traces of certain expressions involving a surface operator, evaluated along the imaginary frequency axis. The surface operator consists of linear combinations with constant coefficients of free Green tensors of the em field of $N + 1$ *homogeneous* infinite media, having the permittivities of the N bodies, and of the medium surrounding them. A potential problem with the approach of [42] is that the expression for the Casimir interaction contains the inverse of the surface operator, that has to be computed numerically by replacing the continuous surfaces with a suitable discrete mesh. This operation replaces the surface operator by a large matrix whose elements involve double surface integrals of the free Green tensors over all pairs of small surface elements composing the mesh. The generation of the matrix is time consuming, because of the strong inverse-distance cubed singularity of the surface operator in the coincidence limit. In addition to that, the size of the non-sparse matrix for sufficiently fine meshes can quickly exceed the memory-usage limit, preventing its numerical inversion.

Inspired by older work by Balian and Duplantier on the Casimir effect for perfect conductors [45,46], we have recently derived a multiple scattering expansion (MSE) of Casimir and CP interactions for magneto-dielectric bodies of arbitrary shape [47,48]. Similar to Ref. [42], in our approach the interactions have the form of traces of expressions involving the inverse of a surface operator $\mathbb{M}(i\zeta)$, evaluated along the imaginary frequency axis. A crucial difference with respect to Ref. [42] is that our kernel \mathbb{M} has the form of a Fredholm surface integral operator of the second kind,

$$\mathbb{M} = \mathbb{I} - \mathbb{K} . \quad (1)$$

The Fredholm form implies that the inverse \mathbb{M} can be computed as a power (Neumann) series

$$\mathbb{M}^{-1} = \mathbb{I} + \mathbb{K} + \mathbb{K}^2 + \dots, \quad (2)$$

which converges provided that the spectral radius of \mathbb{K} is less than one. Hence, we obtain an expansion of Casimir and CP interaction in powers of \mathbb{K} , which can be physically interpreted as an expansion in the number of scatterings off the surfaces of the bodies. Specifically, the MSE has the form of an iterated series of surface integrals of elementary functions, running over the surfaces of the bodies. We note that a particular choice of free coefficients in the kernel \mathbb{K} exists, such that it has a weak $1/|\mathbf{u} - \mathbf{u}'|$ singularity. This should simplify and accelerate numerical evaluations on a mesh. An additional advantage implied by the MSE, if implemented on a mesh, is that one does not need to store the matrix for \mathbb{K} in memory, since its elements can be computed at the moment of performing the matrix multiplication.

In [47] we showed that only a few terms of the MSE are sufficient to obtain a fairly accurate estimate of the Casimir energy between a Si wedge and a Au plate. The purpose of the present work is to investigate the convergence properties of the MSE for the CP interaction between a polarizable isotropic particle and a dielectric body. We use as benchmarks two shapes that can be solved exactly by using the scattering approach, namely a sphere or a cylinder. We consider different types of materials for the sphere and the cylinder, in order to see how the material properties of the bodies affect the rate of convergence of the MSE. We demonstrate that in all cases the MSE converges fast and uniformly with respect to the particle-surface separation. Since there is no reason to expect that the convergence properties of the MSE will be any different for bodies that are smooth deformations of a sphere or a cylinder, we argue that the findings of this work imply that the MSE can be used to efficiently compute the CP interactions for compact and non-compact dielectric bodies with smooth surfaces of any shape.

2. MSE of the scattering Green tensor

Consider a collection of N magneto-dielectric bodies with surfaces S_σ ($\sigma = 1, \dots, N$), characterized by frequency dependent electric and magnetic permeabilities $\epsilon_\sigma(\omega)$ and $\mu_\sigma(\omega)$, respectively, embedded in a homogeneous medium with permittivities $\epsilon_0(\omega)$ and $\mu_0(\omega)$, and let \mathbb{G} is the N -body EM Green tensor. We define the scattering Green tensor $\Gamma(\mathbf{r}, \mathbf{r}')$ as

$$\Gamma(\mathbf{r}, \mathbf{r}') = \mathbb{G}(\mathbf{r}, \mathbf{r}') - \mathbb{G}_0(\mathbf{r}, \mathbf{r}') \quad (3)$$

where \mathbb{G} is the N -body EM Green tensor and \mathbb{G}_0 is the empty space Green tensor for a homogenous medium with contrast ϵ_0, μ_0 (see App. E of [48] for the definition of \mathbb{G}_0). Physically, $\Gamma(\mathbf{r}, \mathbf{r}')$ describes the *modification* of the EM field at position \mathbf{r} due to the presence of the bodies, i.e. the scattered field generated by a source $(\mathbf{J}(\mathbf{r}'), \mathbf{M}(\mathbf{r}'))$ at position \mathbf{r}' outside the bodies. In the surface-integral approach, one imagines that the scattered field at \mathbf{r} is radiated by fictitious tangential electric and magnetic surface currents $(\mathbf{j}_\sigma(\mathbf{u}), \mathbf{m}_\sigma(\mathbf{u}))$ located at points \mathbf{u} on the surfaces of the bodies. One can show [48] that the surface currents satisfy the following set of Fredholm integral equations of the second kind,

$$\sum_{\sigma'=1}^N \int_{S_{\sigma'}} ds_{\mathbf{u}'} [\mathbb{I} - \mathbb{K}_{\sigma\sigma'}(\mathbf{u}, \mathbf{u}')] (\mathbf{j}_{\mathbf{m}_{\sigma'}}^i)(\mathbf{u}') = \int d\mathbf{r} \mathbb{M}_\sigma(\mathbf{u}, \mathbf{r}) (\mathbf{J}_{\mathbf{M}}^i)(\mathbf{r}). \quad (4)$$

In the above Equation, $\mathbb{K}_{\sigma\sigma'}(\mathbf{u}, \mathbf{u}')$ and $\mathbb{M}_{\sigma\sigma'}(\mathbf{u}, \mathbf{u}')$ denote the surface scattering operator (SSO)

$$\mathbb{K}_{\sigma\sigma'}(\mathbf{u}, \mathbf{u}') = 2\mathbb{P}(\mathbb{C}_\sigma^i + \mathbb{C}_\sigma^e)^{-1} \mathbf{n}_\sigma(\mathbf{u}) \times \left[\delta_{\sigma\sigma'} \mathbb{C}_\sigma^i \mathbb{G}_\sigma(\mathbf{u}, \mathbf{u}') - \mathbb{C}_\sigma^e \mathbb{G}_0(\mathbf{u}, \mathbf{u}') \right], \quad \mathbb{P} = \begin{pmatrix} 0 & -1 \\ 1 & 0 \end{pmatrix} \quad (5)$$

and the operator

$$\mathbb{M}_\sigma(\mathbf{u}, \mathbf{r}) = -2\mathbb{P}(\mathbb{C}_\sigma^i + \mathbb{C}_\sigma^e)^{-1} \mathbb{C}_\sigma^e \mathbf{n}_\sigma(\mathbf{u}) \times \mathbb{G}_0(\mathbf{u}, \mathbf{r}). \quad (6)$$

where $\mathbf{n}_\sigma(\mathbf{u})$ is the outward unit normal vector at point \mathbf{u} , and $\delta_{\sigma\sigma'}$ is the Kronecker delta. The operators \mathbb{K} and \mathbb{M} act on electric and magnetic tangential surface fields at \mathbf{u}' . The action of $\mathbf{n}_\sigma(\mathbf{u}) \times$ on the 3×3 matrices $\mathbb{G}_\sigma^{(pq)}$ and $\mathbb{G}_0^{(pq)}$ ($p, q \in \{E, H\}$) are respectively defined by $(\mathbf{n}_\sigma(\mathbf{u}) \times \mathbb{G}_\sigma^{(pq)})\mathbf{v} \equiv \mathbf{n}_\sigma(\mathbf{u}) \times (\mathbb{G}_\sigma^{(pq)}\mathbf{v})$ and $(\mathbf{n}_\sigma(\mathbf{u}) \times \mathbb{G}_0^{(pq)})\mathbf{v} \equiv \mathbf{n}_\sigma(\mathbf{u}) \times (\mathbb{G}_0^{(pq)}\mathbf{v})$, for any vector \mathbf{v} . We note that \mathbb{K} and \mathbb{M} depend on $4N$ arbitrary coefficients, which must form $2N$ invertible diagonal 2×2 matrices $\mathbb{C}_\sigma^i, \mathbb{C}_\sigma^e$. Uniqueness of the surface currents implies that for all choices of these coefficients, the currents solving Eq. (4) for given sources $(\mathbf{J}(\mathbf{r}'), \mathbf{M}(\mathbf{r}'))$ are the same.

The previous considerations imply that the scattering Green tensor has the representation

$$\Gamma(\mathbf{r}, \mathbf{r}') = \int_S ds_{\mathbf{u}} \int_S ds_{\mathbf{u}'} \mathbb{G}_0(\mathbf{r}, \mathbf{u})(\mathbb{I} - \mathbb{K})^{-1}(\mathbf{u}, \mathbf{u}')\mathbb{M}(\mathbf{u}', \mathbf{r}') \quad (7)$$

where the integration extends over all surfaces S_σ and a summation over all surface labels σ is understood. The existence of a MSE follows from the Fredholm type of the operator $(\mathbb{I} - \mathbb{K})^{-1}$ that permits an expansion in powers of \mathbb{K} .

3. Casimir-Polder energy of a polarizable particle and a magneto-dielectric body

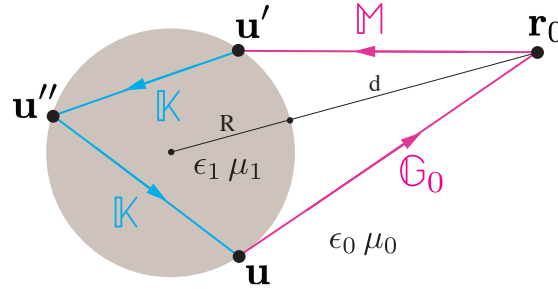


Figure 1. Configuration of a dielectric body (sphere, cylinder) of radius R with electric and magnetic permeabilities ϵ_1, μ_1 , interacting with a polarizable particle at position \mathbf{r}_0 outside the object at a distance d from the surface. The electric and magnetic permeabilities of the surrounding medium are ϵ_0, μ_0 . Shown are also the operators of the multiple scattering expansion, see text for details.

We consider now the Casimir-Polder interaction between a polarizable particle and a magneto-dielectric body, see Fig. 1. We assume that the particle is characterized by a frequency dependent electric polarizability tensor $\alpha(\omega)$ and a magnetic polarizability tensor $\beta(\omega)$. The classical energy of an induced dipole is then given by

$$E_{\text{cl}} = -\frac{1}{2} \sum_{i,j=1}^3 [\alpha_{ij} E_i E_j + \beta_{ij} H_i H_j]. \quad (8)$$

Using the fluctuation-dissipation theorem, this expression is averaged over EM field fluctuations. After removing a divergent contribution from empty space, the Casimir Polder energy is expressed in terms of the scattering Green tensor as

$$E_{\text{CP}} = -4\pi k_B T \sum_{n=0}^{\infty} \kappa_n \sum_{i,j=1}^3 \left[\alpha_{ij}(i\zeta_n) \Gamma_{ij}^{(EE)}(\mathbf{r}_0, \mathbf{r}_0; \kappa_n) + \beta_{ij}(i\zeta_n) \Gamma_{ij}^{(HH)}(\mathbf{r}_0, \mathbf{r}_0; \kappa_n) \right], \quad (9)$$

where k_B is Boltzmann constant, T is the temperature, $\zeta_n = 2\pi n k_B T / \hbar$, $n = 0, 1, 2, \dots$ are the Matsubara frequencies, $\kappa_n = \zeta_n / c$, the prime in the sum indicates that the $n = 0$ terms

has to be taken with a weight of $1/2$, and \mathbf{r}_0 is the particle's position. Substitution of Γ from Eq. (7) yields the interaction energy of the particle with the body in terms of the SSO. This energy can be computed by a MSE with respect to the number of scatterings at the surface of the body. It is instructive to consider explicitly the first terms of the scattering expansion of the Casimir-Polder energy, assuming for simplicity that the electric polarizability of the particle is isotropic $\alpha_{ij} = \alpha \delta_{ij}$, and that its magnetic polarizability β is negligible, yielding

$$E_{\text{CP}} = -4\pi k_B T \sum_{n=0}^{\infty} \kappa_n \alpha (i \zeta_n) \left\{ \sum_{p=E,H} \int_S ds_{\mathbf{u}} \text{tr} \left[\mathbb{G}_0^{(Ep)}(\mathbf{r}_0, \mathbf{u}; \kappa_n) \mathbb{M}^{(pE)}(\mathbf{u}, \mathbf{r}_0; \kappa_n) \right] \right. \\ \left. + \sum_{p,q=E,H} \int_S ds_{\mathbf{u}} \int_S ds_{\mathbf{u}'} \text{tr} \left[\mathbb{G}_0^{(Ep)}(\mathbf{r}_0, \mathbf{u}; \kappa_n) \mathbb{K}^{(pq)}(\mathbf{u}, \mathbf{u}'; \kappa_n) \mathbb{M}^{(qE)}(\mathbf{u}', \mathbf{r}_0; \kappa_n) \right] \right\} + \dots \quad (10)$$

where tr denotes a trace over tensor spatial indices. Recalling that the kernels \mathbb{K} and \mathbb{M} are combinations of free-space Green tensors \mathbb{G}_0 and \mathbb{G}_σ , and that the latter are elementary functions, we see from the above equation that the CP energy is expressed in terms of iterated integrals of elementary functions extended on the surface S of the body. Since for imaginary frequencies the Green tensors decay exponentially with distance, Eq. (10) makes evident the intuitive fact that the points of the surface that are closest to the particle dominate the interaction. However, for the classical term $n = 0$ the Matsubara frequency vanishes, and the operators decay only according to a power law.

4. Equivalent formulations of the SSO

With different interior coefficient matrices \mathbb{C}_σ^i and exterior coefficient matrices \mathbb{C}_σ^e the SSO form an equivalence class of operators in the sense that Eq. (4) yields the same surface currents for a given external source for all coefficients, as long as neither the interior nor the exterior matrices vanish for any σ , and the sum $\mathbb{C}_\sigma^i + \mathbb{C}_\sigma^e$ is invertible. Consequently, the scattering Green tensor and the CP energy must be also independent of the choice made for the coefficients. The surface currents and the Casimir energy at any *finite* order of the MSE, however, in general do depend on the chosen coefficients, and hence does the rate of convergence of the MSE. This remarkable property provides an effective method to optimize convergence for different permittivities and even frequencies by suitable adjustment of coefficients. Among the infinitely many choices there are two which we consider important to discuss explicitly:

(C1) In general, the SSO has a leading singularity that diverges as $1/|\mathbf{u} - \mathbf{u}'|^\gamma$ with $\gamma = 3$ when the two surface positions \mathbf{u}, \mathbf{u}' approach each other. There exists a choice of coefficients [49], however, for which the singularity is reduced to a weaker divergence with exponent $\gamma = 1$. The coefficient matrices are

$$\mathbb{C}_\sigma^i = \text{diag}(\epsilon_\sigma, \mu_\sigma), \quad \mathbb{C}_\sigma^e = \text{diag}(\epsilon_0, \mu_0). \quad (11)$$

The corresponding surface operator \mathbb{K} has unique mathematical properties (see Sec. VI of [48]).

(C2) A fully asymmetric, material independent choice of coefficient matrices is

$$\mathbb{C}_\sigma^i = \text{diag}(1, 0), \quad \mathbb{C}_\sigma^e = \text{diag}(0, 1). \quad (12)$$

5. Results and Discussion

The MSE of the CP energy Eq. (10) converges if all eigenvalues of the SSO \mathbb{K} are less than one in modulus, which we call the boundedness property. Unfortunately, we have not been able to derive a general bound on the eigenvalues of \mathbb{K} . However, we could prove [48] the boundedness property for the choice (C1) of the coefficients [see Eq. (11)] in the asymptotic limit of infinite frequencies for bodies of any shape. For compact bodies, the boundedness property holds also in the static limit $\kappa = 0$. For the special case of perfect

conductors of compact shape, the boundedness property was proven long time ago at all frequencies [45].

While having a proof of convergence of the MSE is clearly desirable, from the practical point of view it is more important to know if convergence is fast enough that the first few terms of the MSE provide a good approximation to the complete series. Given the current status of experiments, getting the CP energy with an error less than say a percent would be good enough. To investigate this problem, we thought of using as a benchmark the CP interaction of a particle with a body for which the scattering amplitude (T-matrix) is exactly known, and then to verify in such a setup the rate of convergence of the MSE expansion to the exact energy. We chose to study a dielectric sphere and a dielectric cylinder. We consider three different materials, representing a conductor (gold), a semiconductor (silicon) and an insulator (polystyrene). Since these materials have widely different permittivities, we can check how the rate of convergence of the MSE is affected by the magnitude of the permittivity. We have compared the rate of convergence of the MSE for the two choices (C1) and (C2) of the free coefficients that enter in the definition of the SSO. We shall denote by MSE_k , $k = 0, 1, \dots$ the estimate of the CP energy corresponding to including up-to k powers of \mathbb{K} in the MSE of Eq. (9).

5.1. Materials

In our computations we used for the permittivities of the materials the expressions

$$\epsilon_{\text{Au}}(i\zeta_n) = 1 + \frac{\Omega_p^2}{\zeta(\zeta + \gamma)} + \sum_j \frac{f_j}{\omega_j^2 + g_j\zeta + \zeta^2}, \quad (13)$$

$$\epsilon_{\text{Si}}(i\zeta_n) = \epsilon_\infty^{(\text{Si})} + \frac{\epsilon_0^{(\text{Si})} - \epsilon_\infty^{(\text{Si})}}{1 + \zeta^2/\omega_{\text{UV}}^2}, \quad (14)$$

$$\epsilon_{\text{polystyrene}}(i\zeta_n) = 1 + \sum_j \frac{f_j}{\omega_j^2 + g_j\zeta + \zeta^2}, \quad (15)$$

where $\Omega_p = 9 \text{ eV}/\hbar$, $\gamma = 0.035 \text{ eV}/\hbar$, $\epsilon_\infty^{(\text{Si})} = 1.035$, $\epsilon_0^{(\text{Si})} = 11.87$, $\omega_{\text{UV}} = 4.34 \text{ eV}/\hbar$, and the oscillator parameters ω_j, f_j, g_j for Au and polystyrene are listed in Tables (1) and (2) respectively. We assume that the particle's polarizability α is frequency independent.

5.2. CP energy for a sphere

The scattering approach yields for the CP interaction energy of a polarizable particle at distance d from the surface of a sphere of radius R in vacuum ($\epsilon_0 = \mu_0 = 1$) the result

$$E_{\text{CP}}^{(\text{exact})} = \frac{k_B T}{a^2} \sum_{n=0}^{\infty} \kappa_n \alpha(i\zeta_n) \sum_{l=1}^{\infty} (2l+1) \times \left\{ T_l^{\text{HH}}(i\zeta_n) \mathcal{K}_l^2(\kappa_n a) - T_l^{\text{EE}}(i\zeta_n) \left[\mathcal{K}_l'^2(\kappa_n a) + \frac{l(l+1)}{\kappa_n^2 a^2} \mathcal{K}_l^2(\kappa_n a) \right] \right\}, \quad (16)$$

where $a = R + d$, l is the multipole index, $\mathcal{K}_l'(x) = d\mathcal{K}_l/dx$, $\mathcal{K}_l(x) = xk_l(x)$, $k_l(x) = \sqrt{\frac{2}{\pi x}} K_{l+1/2}(x)$ is the modified spherical Bessel function of the third kind, and $T_l^{\text{HH}}, T_l^{\text{EE}}$ are the T-matrix elements (Mie coefficients) of the sphere,

$$T_l^{\text{HH}}(i\zeta) = \frac{\sqrt{\mu/\epsilon} \mathcal{I}_l(\sqrt{\epsilon\mu}\kappa R) \mathcal{I}_l'(\kappa R) - \mathcal{I}_l'(\sqrt{\epsilon\mu}\kappa R) \mathcal{I}_l(\kappa R)}{\mathcal{K}_l(\kappa R) \mathcal{I}_l'(\sqrt{\epsilon\mu}\kappa R) - \sqrt{\mu/\epsilon} \mathcal{I}_l(\sqrt{\epsilon\mu}\kappa R) \mathcal{K}_l'(\kappa R)}, \quad (17)$$

$$T_l^{\text{EE}}(i\zeta) = \frac{\sqrt{\epsilon/\mu} \mathcal{I}_l(\sqrt{\epsilon\mu}\kappa R) \mathcal{I}_l'(\kappa R) - \mathcal{I}_l'(\sqrt{\epsilon\mu}\kappa R) \mathcal{I}_l(\kappa R)}{\mathcal{K}_l(\kappa R) \mathcal{I}_l'(\sqrt{\mu/\epsilon}\kappa R) - \sqrt{\epsilon/\mu} \mathcal{I}_l(\sqrt{\epsilon\mu}\kappa R) \mathcal{K}_l'(\kappa R)}, \quad (18)$$

$$T_l^{\text{EH}}(i\zeta) = T_l^{\text{HE}}(i\zeta) = 0, \quad (19)$$

where $\xi = \kappa c$, $\mathcal{I}_l(x) = x i_l(x)$ and $\mathcal{I}'_l(x) = d\mathcal{I}_l/dx$ with $i_l(x) = \sqrt{\frac{\pi}{2x}} I_{l+1/2}(x)$ the modified spherical Bessel function of the first kind.

The matrix elements of the SSO \mathbb{K} and the operator \mathbb{M} can be easily computed in the basis of vector spherical harmonics. The corresponding matrices are both diagonal with respect to multipole indices (l, m) ($-l \leq m \leq l$), and in addition they are independent of m . Therefore, the matrix for \mathbb{K} has the structure of l -dependent 4×4 blocks $K_{p,r,l,m;q,s,l',m'} = \delta_{ll'} \delta_{mm'} K_{p,r;q,s}^{(l)}$, where $p, q = E, H$ and $r, s = 1, 2$ label the tangential fields $Y_{1,lm}(\hat{r})$ and $Y_{2,lm}(\hat{r})$ introduced in Eq. (8.1) of [46].

In Figs. 2-4 we show plots of the ratios of the MSE for the CP energy $E_{\text{CP}}^{(\text{MSE}_k)}$ and the exact result for the CP energy $E_{\text{CP}}^{(\text{exact})}$ obtained from Eq. (16) versus d/R for Au, Si and polystyrene. In the case of Au, a comparison of Fig. 2(a) with Fig. 2(b) shows that the rate of convergence is much faster with the asymmetric choice (C2) of the coefficients. In fact, with the (C2) choice already MSE_3 differs from the exact energy by less than one percent for all displayed separations: specifically, the maximum error is of 0.6% for $d/R = 1$, while for $d/R = 0.03$ the error is as small as 0.1 %. In the case of Si, the performance of the choice (C1) is better than (C2). Indeed, with the (C1) choice the maximum error of MSE_4 is of 0.8% for $d/R = 0.03$ while the minimum error is of 0.2 % for $d/R = 1$, while for the choice (C2) the maximum error is of 3.4% for $d/R = 1$. In the case of polystyrene, the performance of the (C1) is excellent, since with MSE_3 the maximum error is of 0.6 % for $d/R = 1$, while for $d/R = 0.04$ the error is as low as 0.003 %. For polystyrene, the rate of convergence of (C2) is instead very poor.

Table 1. Oscillator parameters for Au [50]

ω_j (eV/ \hbar)	f_j (eV ² / \hbar^2)	g_j (eV/ \hbar)
3.05	7.091	0.75
4.15	41.46	1.85
5.4	2.7	1.0
8.5	154.7	7.0
13.5	44.55	6.0
21.5	309.6	9.0

Table 2. Oscillator parameters for polystyrene [4]

ω_j (eV/ \hbar)	f_j (eV ² / \hbar^2)	g_j (eV/ \hbar)
6.35	14.6	0.65
14.0	96.9	5.0
11.0	44.4	3.5
20.1	136.9	11.5

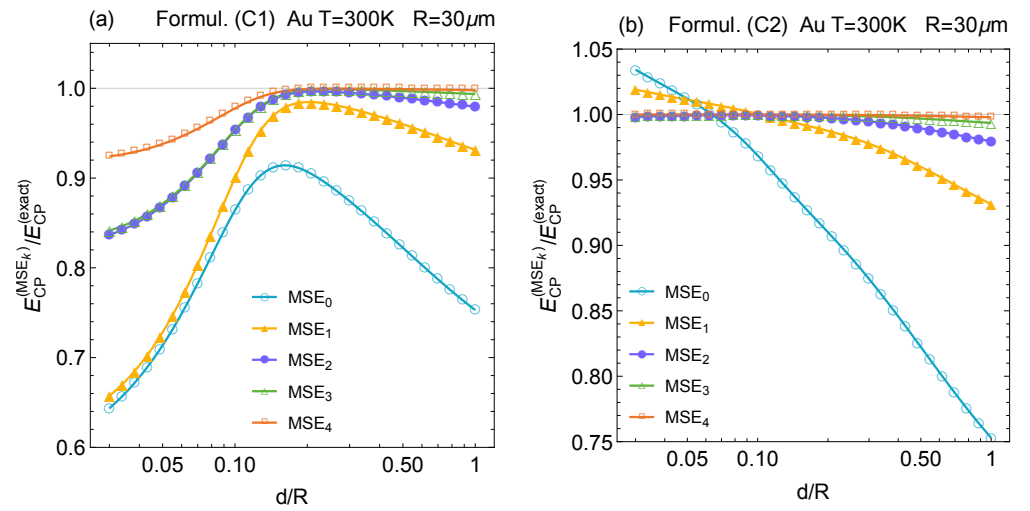


Figure 2. MSE of the CP energy for a Au sphere of radius $R = 30 \mu\text{m}$ at room temperature: (a) for the formulation (C1), (b) for the formulation (C2).

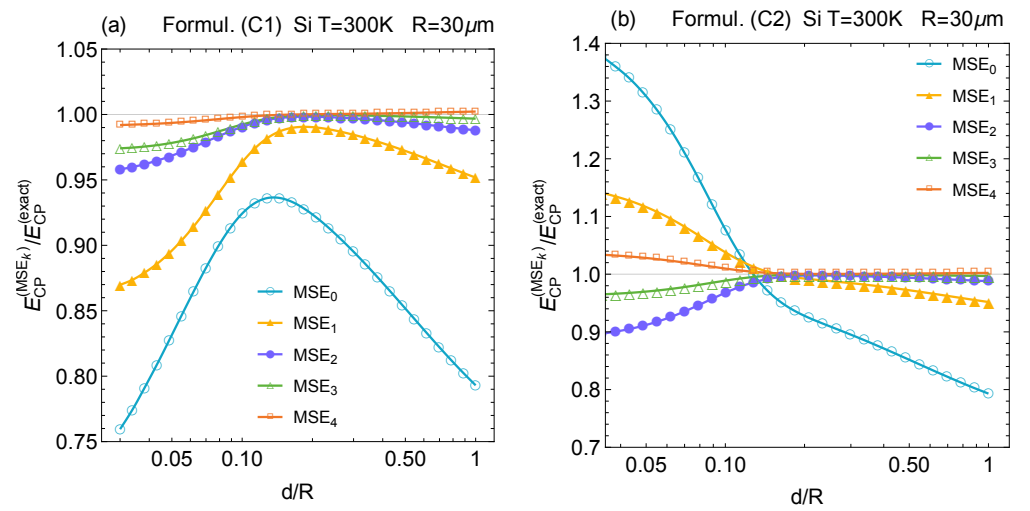


Figure 3. MSE of the CP energy for a Si sphere of radius $R = 30 \mu\text{m}$ at room temperature: (a) for the formulation (C1), (b) for the formulation (C2).

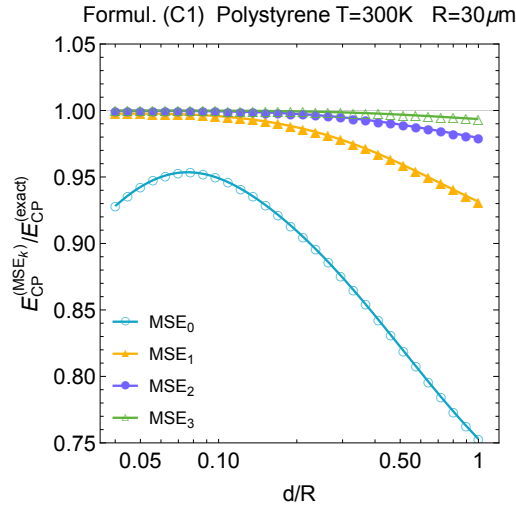


Figure 4. MSE of the CP energy for a polystyrene sphere of radius $R = 30 \mu\text{m}$ at room temperature, for the formulation (C1).

5.3. CP energy for a cylinder

Within the scattering T-matrix approach, the CP interaction energy of a polarizable particle at distance d from the surface of an infinitely long cylinder of radius R with electric and magnetic permeabilities $\epsilon_1 = \epsilon$, $\mu_1 = \mu$ in vacuum ($\epsilon_0 = \mu_0 = 1$) is

$$\begin{aligned}
 E_{\text{CP}}^{(\text{exact})} &= \frac{k_B T}{\pi} \sum_{n=0}^{\infty} \kappa_n^2 \alpha(i\zeta_n) \int_{-\infty}^{\infty} dk_z \sum_{m=-\infty}^{\infty} \\
 &\times \left\{ T_{k_z m}^{\text{EE}}(i\zeta_n) \frac{1}{\kappa_n^2} \left[k_z^2 K_m'^2(p_0 a) + \left(\frac{m^2 k_z^2}{p_0^2 a^2} + p_0^2 \right) K_m^2(p_0 a) \right] \right. \\
 &- T_{k_z m}^{\text{HH}}(i\zeta_n) \left[K_m'^2(p_0 a) + \frac{m^2}{p_0^2 a^2} K_m^2(p_0 a) \right] \\
 &\left. + T_{k_z m}^{\text{EH}}(i\zeta_n) \frac{4mk_z}{\kappa_n p_0 a} K_m(p_0 a) K_m'^2(p_0 a) \right\}, \quad (20)
 \end{aligned}$$

where $a = R + d$, $p_0 = \sqrt{\kappa^2 + k_z^2}$, m is the multipole index, K_m is the modified Bessel function of second kind and K_m' its derivative, and $T_{k_z m}^{NM}$, ($N, M \in \{E, H\}$) are the T-matrix elements of a dielectric cylinder [51],

$$T_{k_z m}^{\text{HH}}(i\zeta) = -\frac{I_m(p_0 R)}{K_m(p_0 R)} \frac{\Delta_1 \Delta_4 + Y^2}{\Delta_1 \Delta_2 + Y^2}, \quad (21)$$

$$T_{k_z m}^{\text{EE}}(i\zeta) = -\frac{I_m(p_0 R)}{K_m(p_0 R)} \frac{\Delta_2 \Delta_3 + Y^2}{\Delta_1 \Delta_2 + Y^2}, \quad (22)$$

$$T_{k_z m}^{\text{HE}}(i\zeta) = -T_{k_z m}^{\text{EH}}(i\zeta) = \frac{Y}{\sqrt{\epsilon\mu}(p_0 R)^2 K_m(p_0 R)^2} \frac{1}{\Delta_1 \Delta_2 + Y^2}, \quad (23)$$

with I_m the modified Bessel function of first kind, and

$$Y = \frac{mk_z}{\sqrt{\epsilon\mu}R^2\kappa} \left(\frac{1}{p^2} - \frac{1}{p_0^2} \right), \quad (24)$$

with $p = \sqrt{\epsilon\mu\kappa^2 + k_z^2}$ and

$$\Delta_1 = \frac{I'_m(pR)}{pRI_m(pR)} - \frac{1}{\epsilon} \frac{K'_m(p_0R)}{p_0RK_m(p_0R)}, \quad (25)$$

$$\Delta_2 = \frac{I'_m(pR)}{pRI_m(pR)} - \frac{1}{\mu} \frac{K'_m(p_0R)}{p_0RK_m(p_0R)}, \quad (26)$$

$$\Delta_3 = \frac{I'_m(pR)}{pRI_m(pR)} - \frac{1}{\epsilon} \frac{I'_m(p_0R)}{p_0RI_m(p_0R)}, \quad (27)$$

$$\Delta_4 = \frac{I'_m(pR)}{pRI_m(pR)} - \frac{1}{\mu} \frac{I'_m(p_0R)}{p_0RI_m(p_0R)}. \quad (28)$$

Notice that in general the polarization is *not conserved* under scattering, i.e., $T_{k_z m}^{EH} \neq 0 \neq T_{k_z m}^{HE}$. This property, together with its quasi-2D shape, makes the cylinder an important benchmark test for the convergence of the MSE.

The CP energy can be easily obtained as a MSE since the SSO \mathbb{K} and the operator \mathbb{M} can be computed by substituting for the free Green functions in Eqs. (5), (6) an expansion in vector cylindrical waves. In Fig. 5 we show again numerical results for the ratio of the MSE for the CP energy $E_{\text{CP}}^{(\text{MSE}_k)}$ at MSE order k and the exact result for the CP energy $E_{\text{CP}}^{(\text{exact})}$ obtained from Eq. (21). The materials, temperature and geometric lengths are the same as in the case of a sphere. For Si we observe that the MSE with choice (C1) has converged at order MSE₃ to the exact energy within about 3%, with the largest deviations at the shortest (2.4%) and longest considered (3.3%) separation. The deviation is minimal at intermediate distances around $d/R = 0.2$ with an error of only 0.1%. Hence the performance of the MSE for an infinite cylinder is very similar to a compact sphere. We did not consider the coefficients (C2) as they performed worse than choice (C1) for a sphere. For polystyrene we consider again only the choice (C1), for the same reason. Due to its low dielectric contrast, we expect the choice (C1) to give excellent convergence of the MSE at low order. Indeed, the rate of convergence is so fast that the MSE can be terminated at order MSE₁ already, with a maximum deviation from the exact energy of only 1.9% at the separation $d = R$. In general, we note that with the choice (C1) the lowest order MSE₀ the estimate of the energy for the cylinder is less good than for the sphere. This is presumably due to arbitrarily long range charge and current fluctuations along the cylinder which require at least one power the operator \mathbb{K} to be described properly.

Finally, it is important to discuss the case of a metal, like Au. As the dielectric function diverges in the limit $\kappa \rightarrow 0$, the classical term $n = 0$ of the Matsubara sum resembles that of a perfect conductor. We had shown that for a cylinder the SSO \mathbb{K} , for the choice (C1), in the partial wave channel $m = 0$ has an eigenvalue that approaches unity when $\kappa \rightarrow 0$ and $\epsilon \rightarrow \infty$ [48]. For the choice (C2) the situation is even worse as there is an eigenvalue approaching unity in all partial wave channels. We expect this property to persist for all quasi-2D shapes with a compact cross section. Hence, for such metallic shapes the classical term $n = 0$ cannot be obtained from a MSE. However, our surface scattering approach is also useful for zero frequency $\kappa = 0$ as the inverse of $\mathbb{M} = \mathbb{I} - \mathbb{K}$ can be computed directly, without resorting to a MSE. We note that for $\kappa = 0$ the expression for \mathbb{K} simplifies considerably, in particular in the perfect conductor limit [48].

To conclude, we have demonstrated that the MSE provides an excellent device to compute Casimir-Polder interactions with high precision for a wide range of materials. We stress that this conclusion is not specific to the shapes considered here but is expected to hold generically for any compact 3D shape or quasi-2D shape. Here we considered a sphere and a cylinder only for the reason that for those shapes exact results are known and hence the convergence of our MSE can be tested. Most importantly, for general shapes where the T-matrix is not known, the SSO \mathbb{K} can be computed and the MSE implemented to obtain high precision results for the interaction.

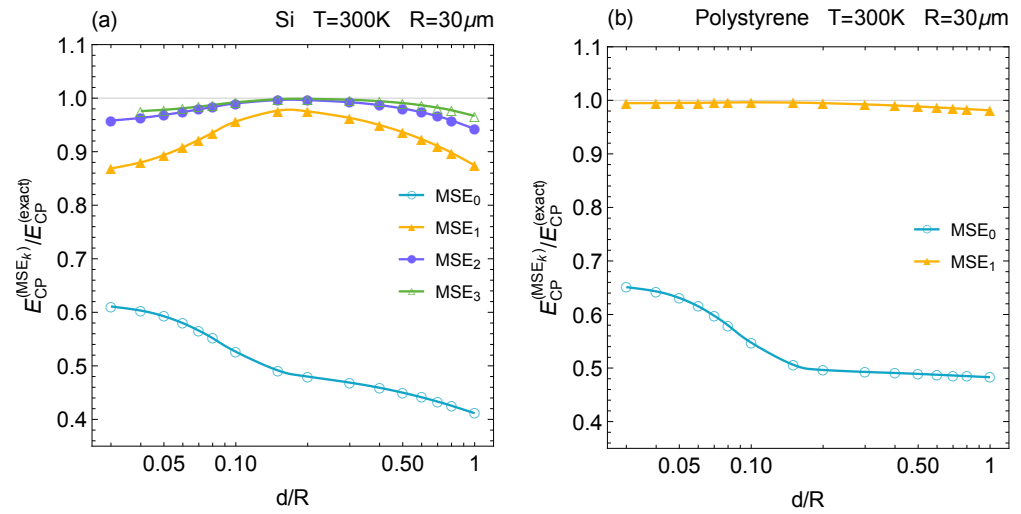


Figure 5. MSE of the CP energy for (a) a Silicon cylinder and (b) a polystyrene cylinder of radius $R = 30 \mu\text{m}$ at room temperature $T = 300\text{K}$, for the formulation (C1).

1. Casimir, H.B.G. On the attraction between two perfectly conducting plates. *Proc. K. Ned Akad. Wet* **1948**, *51*, 793.
2. Lifshitz, E.M. The theory of molecular attractive force between solids. *Sov. Phys. J. Exp Theoret. Phys* **1956**, *2*, 73.
3. Derjaguin, B.V.; Abrikosova, I.I. Direct measurement of the molecular attraction of solid bodies. 1. Statement of the problem and method of measuring forces by using negative feedback. *Sov. Phys. J. Exp. Theoret. Phys* **1957**, *3*, 819–829.
4. Parsegian, V.A. *Van der Waals forces: a handbook for biologists, chemists, engineers, and physicists*; Cambridge University Press, 2006.
5. Klimchitskaya, G.L.; Mohideen, U.; Mostepanenko, V.M. The Casimir force between real materials: experiment and theory. *Rev. Mod. Phys.* **2009**, *81*, 1827.
6. Buhmann, S.Y. *Dispersion Forces I : Macroscopic Quantum Electrodynamics and ground-state Casimir, Casimir-Polder, and van der Waals forces*; Springer: Berlin, 2012.
7. Rodriguez, A.W.; Hui, P.C.; Woolf, D.P.; Johnson, S.G.; Loncar, M.; Capasso, F. Classical and fluctuation-induced electromagnetic interactions in micron-scale systems: designer bonding, antibonding, and Casimir forces. *Annalen Physik* **2014**, *527*, 45.
8. Woods, L.M.; Dalvit, D.A.R.; Tkatchenko, A.; Rodriguez-Lopez, P.; Rodriguez, A.W.; Podgornik, R. Materials perspective on Casimir and van der Waals interactions. *Rev. Mod. Phys.* **2016**, *88*, 045003.
9. Bimonte, G.; Emig, T.; Kardar, M.; Krüger, M. Nonequilibrium fluctuational Quantum Electrodynamics: heat radiation, heat transfer, and force. *Annu. Rev. Condens. Matter Phys.* **2017**, *8*, 119–143.
10. Bimonte, G.; Emig, T.; Graham, N.; Kardar, M. Something can come of nothing: surface approaches to Quantum fluctuations and the Casimir force. *Ann. Rev. Nuc. Part. Sci.* **2022**, *72*, 93 – 118.
11. Langbein, D. *Theory of van der Waals Attraction*; Springer, 1974.
12. Lamoreaux, S.K. Demonstration of the Casimir force in the 0.6 to 6 μm range. *Phys. Rev. Lett.* **1997**, *78*, 5.
13. Mohideen, U.; Roy, A. Precision Measurement of the Casimir Force from 0.1 to 0.9 μm . *Phys. Rev. Lett.* **1998**, *81*, 4549.
14. Chan, H.B.; Aksyuk, V.A.; Kleiman, R.N.; Bishop, D.J.; Capasso, F. Quantum mechanical actuation of microelectromechanical systems by the Casimir force. *Science* **2001**, *291*, 1941.
15. Bressi, G.; Carugno, G.; Onofrio, R.; Ruoso, G. Measurement of the Casimir force between parallel metallic surfaces. *Phys. Rev. Lett.* **2002**, *88*, 041804.
16. Decca, R.S.; López, D.; Fischbach, E.; Krause, D.E. Measurement of the Casimir force between dissimilar metals. *Phys. Rev. Lett.* **2003**, *91*, 050402.

17. Munday, J.N.; Capasso, F.; Parsegian, V.A. Measured long-range repulsive Casimir–Lifshitz forces. *Nature* **2009**, *457*, 170.
18. Sushkov, A.O.; Kim, W.J.; Dalvit, D.A.R.; Lamoreaux, S.K. Observation of the thermal Casimir force. *Nat. Phys.* **2011**, *7*, 230.
19. Tang, L.; Wang, M.; Ng, C.Y.; Nikolic, M.; Chan, C.T.; Rodriguez, A.W.; Chan, H.B. Measurement of non-monotonic Casimir forces between silicon nanostructures. *Nature Photonics* **2017**, *11*, 97–101. <https://doi.org/10.1038/nphoton.2016.254>.
20. Bimonte, G.; López, D.; Decca, R.S. Isoelectronic determination of the thermal Casimir force. *Phys. Rev. B* **2016**, *93*, 184434.
21. Emig, T.; Graham, N.; Jaffe, R.L.; Kardar, M. Casimir forces between arbitrary compact objects. *Phys. Rev. Lett.* **2007**, *99*, 170403.
22. Kenneth, O.; Klich, I. Casimir forces in a T-operator approach. *Phys. Rev. B* **2008**, *78*, 014103.
23. Rahi, S.J.; Emig, T.; Graham, N.; Jaffe, R.L.; Kardar, M. Scattering theory approach to electrodynamic Casimir forces. *Phys. Rev. D* **2009**, *80*, 085021.
24. Genet, C.; Lambrecht, A.; Reynaud, S. Casimir force and the quantum theory of lossy optical cavities. *Phys. Rev. A* **2003**, *67*, 043811. <https://doi.org/10.1103/PhysRevA.67.043811>.
25. Lambrecht, A.; Maia Neto, P.A.; Reynaud, S. The Casimir effect within scattering theory. *New J. Phys.* **2006**, *8*, 243.
26. Maghrebi, M.F.; Rahi, S.J.; Emig, T.; Graham, N.; Jaffe, R.L.; Kardar, M. Analytical results on Casimir forces for conductors with edges and tips. *PNAS* **2011**, *108*, 6867–6871.
27. Bimonte, G.; Emig, T. Exact results for classical Casimir interactions: Dirichlet and Drude model in the sphere-sphere and sphere-plane geometry. *Phys. Rev. Lett.* **2012**, *109*, 160403.
28. Schoger, T.; Ingold, G.L. Classical Casimir free energy for two Drude spheres of arbitrary radii: A plane-wave approach. *Sc Post Phys. Core* **2021**, *4*, 011.
29. Hartmann, M.; Ingold, G.L.; Maia Neto, P.A. Plasma versus Drude Modeling of the Casimir Force: Beyond the Proximity Force Approximation. *Phys. Rev. Lett.* **2017**, *119*, 043901.
30. Wang, M.; Tang, L.; Ng, C.Y.; et al. Strong geometry dependence of the Casimir force between interpenetrated rectangular gratings. *Nature Commun.* **2021**, *12*, 600.
31. Banishev, A.A.; Wagner, J.; Emig, T.; Zandi, R.; Mohideen, U. Demonstration of Angle-Dependent Casimir Force between Corrugations. *Phys. Rev. Lett.* **2013**, *110*, 250403. <https://doi.org/10.1103/PhysRevLett.110.250403>.
32. Intravaia, F.; Koev, S.; Jung, I.W.; Talin, A.A.; Davids, P.S.; Decca, R.S.; Aksyuk, V.A.; Dalvit, D.A.R.; López, D. Strong Casimir force reduction through metallic surface nanostructuring. *Nature Commun.* **2013**, *4*, 2515. <https://doi.org/10.1038/ncomms3515>.
33. Lambrecht, A.; Marachevsky, V.N. Casimir Interaction of Dielectric Gratings. *Phys. Rev. Lett.* **2008**, *101*, 160403.
34. Bender, H.; Stehle, C.; Zimmermann, C.; Slama, S.; Fiedler, J.; Scheel, S.; Buhmann, S.Y.; Marachevsky, V.N. Probing Atom-Surface Interactions by Diffraction of Bose-Einstein Condensates. *Phys. Rev. X* **2014**, *4*, 011029.
35. Antezza, M.; Chan, H.; Guizal, B.; Marachevsky, V.N.; Messina, R.; Wang, M. Giant Casimir Torque between Rotated Gratings and the $\theta = 0$ anomaly. *Phys. Rev. Lett.* **2020**, *124*, 013903.
36. Fosco, C.D.; Lombardo, F.C.; Mazzitelli, F.D. Proximity force approximation for the Casimir energy as a derivative expansion. *Phys.Rev.D* **2011**, *84*, 105031.
37. Bimonte, G.; Emig, T.; Jaffe, R.L.; Kardar, M. Casimir forces beyond the proximity approximation. *Europhys. Lett.* **2012**, *97*, 50001.
38. Bimonte, G.; Emig, T.; Kardar, M. Material dependence of Casimir forces: gradient expansion beyond proximity. *Appl. Phys. Lett.* **2012**, *100*, 074110.
39. Bimonte, G. Going beyond PFA: A precise formula for the sphere-plate Casimir force. *Europhys. Lett.* **2017**, *118*, 20002.
40. Bimonte, G.; Emig, T.; Kardar, M. Casimir-Polder interaction for gently curved surfaces. *Phys. Rev. D* **2014**, *90*, 081702(R).
41. Bimonte, G.; Emig, T.; Kardar, M. Casimir-Polder force between anisotropic nanoparticles and gently curved surfaces. *Phys. Rev. D* **2015**, *92*, 025028.
42. Reid, M.T.H.; White, J.; Johnson, S.G. Fluctuating surface currents: an algorithm for efficient prediction of Casimir interactions among arbitrary materials in arbitrary geometries. *Phys. Rev. A* **2013**, *88*, 022514.
43. Chew, W.; Tong, M. *Integral Equations Methods for Electromagnetic and Elastic Waves*; Synthesis Lectures on Computational Electromagnetics Series, Morgan and Claypool Publishers, 2009.
44. Volakis, S.K. *Integral Equations Methods for Electromagnetics*; SciTech Publishing, 2012.

45. Balian, R.; Duplantier, B. Electromagnetic waves near perfect conductors. I. Multiple scattering expansions. Distribution of modes. *Ann. Phys (NY)* **1977**, *104*, 300–335.
46. Balian, R.; Duplantier, B. Electromagnetic waves near perfect conductors. II. Casimir effect. *Ann. Phys. (NY)* **1978**, *112*, 165–208.
47. Emig, T.; Bimonte, G. Multiple scattering expansion for dielectric Media: Casimir effect. *Phys. Rev. Lett.* **2023**, *130*, 200401.
48. Bimonte, G.; Emig, T. Casimir and Casimir-Polder Interactions for Magneto-dielectric Materials: Surface Scattering Expansion. *Phys. Rev. A* **2023**, *108*, 052807.
49. Müller, C. *Foundations of the mathematical theory of electromagnetic waves*; Springer, 1969.
50. Decca, R.S.; Lopez, D.; Fischbach, E.; Klimchitskaya, G.K.; Krause, D.E.; Mostepanenko, V.M. Novel constraints on light elementary particles and extra-dimensional physics from the Casimir effect. *Eur. Phys. J. C* **2007**, *51*, 963.
51. Noruzifar, E.; Emig, T.; Mohideen, U.; Zandi, R. Collective charge fluctuations and Casimir interactions for quasi-one-dimensional metals. *Phys. Rev. B* **2012**, *86*, 115449.